

FORMING HABITABLE PLANETS AROUND DWARF STARS: APPLICATION TO OGLE-06-109L

SU WANG AND JI-LIN ZHOU

Department of Astronomy & Key Laboratory of Modern Astronomy and Astrophysics in Ministry of Education, Nanjing University,
Nanjing 210093, China, suwang@nju.edu.cn, zhoujl@nju.edu.cn

Draft version October 20, 2018

ABSTRACT

Dwarf stars are believed to have small protostar disk where planets may grow up. During the planet formation stage, embryos undergoing type I migration are expected to be stalled at inner edge of magnetic inactive disk ($a_{\text{crit}} \sim 0.2 - 0.3$ AU). This mechanism makes the location around a_{crit} a sweet spot of forming planets. Especially, a_{crit} of dwarf stars with masses $\sim 0.5 M_{\odot}$ is roughly inside the habitable zone of the system. In this paper we study the formation of habitable planets due to this mechanism with a model system OGLE-06-109L. It has a $0.51 M_{\odot}$ dwarf star with two giant planets in 2.3 and 4.6 AU observed by microlensing. We model the embryos undergoing type I migration in the gas disk with a constant disk accretion rate (\dot{M}). Giant planets in outside orbits affect the formation of habitable planets through secular perturbations at the early stage and secular resonance at the later stage. We find that the existence and the masses of the habitable planets in OGLE-06-10L system depend on both \dot{M} and the speed of type I migration. If planets formed earlier so that \dot{M} is larger ($\sim 10^{-7} M_{\odot} \text{ yr}^{-1}$), terrestrial planet can not be survived unless the type I migration rate is an order of magnitude less. If planets formed later so that \dot{M} is smaller ($\sim 10^{-8} M_{\odot} \text{ yr}^{-1}$), single and high mass terrestrial planets with high water contents ($\sim 5\%$) will be formed by inward migration of outer planet cores. A slower speed migration will result in several planets by collisions of embryos, thus their water contents are low ($\sim 2\%$). Mean motion resonances or apsidal resonances among planets may be observed if multiple planets survived in the inner system.

Subject headings: (stars:) planetary systems: formation – solar system: formation – stars: individual (OGLE-06-109L)

1. INTRODUCTION

One of the interesting problems for planetary dynamics is whether there exist stable orbits in the habitable zone (HZ) of main sequence stars. Earth-size planets in HZ possibly have similar compositions especially liquid water, which is important for life survival (Kasting et al. 1993; Hinse et al. 2008). Currently, radial velocity technique is not sensitive enough to detect terrestrial planets in HZ of ~ 1 AU around solar type stars. However, dwarf stars with masses $\sim 0.5 M_{\odot}$ have very close habitable zones ($\sim 0.2 - 0.3$ AU) due to their low stellar luminosity, thus they are good candidates for terrestrial planets detection in HZ.

According to the simulations of terrestrial planet formation in exoplanet systems, *in site* formation of Earth-size planets in close-in orbits requires a very massive circumstellar disk, e.g., ~ 30 times of minimum solar nebular (Raymond et al. 2008) to form a $\sim 10 M_{\oplus}$ planet around GJ 581. Thus formation of Earth-like planets in close-in orbits requires either keeping adding building blocks into inner orbits, or massive cores formed in outside orbits and migrating inward under, e.g., the type I migration.

If giant planets already formed in outside orbits, perturbations from giant planets that undergo type II migrations may be helpful to the final assembly of terrestrial planets in close-in orbits. During the inward migration of giant planets embedded in the viscous gas disk, the locations of inner mean motion resonances (MMR) with the gas giants, mainly 2:1 MMR, will sweep through the inner disk, trap and shepherd the embryos, and ex-

cite their eccentricities, which results in the mergers of isolated embryos and the formation of close-in planets (Zhou et al. 2005; Fogg & Nelson 2005; Raymond et al. 2006). During the stage of gas disk depletion, secular resonances caused by disk potential and outer giant planets will sweep into the inner region, which may excite the eccentricities of the embryos and results in the merger and formation of exoplanets (Nagasawa et al. 2003; Zhou et al. 2005).

In the above mentioned scenarios, the type I migration of embryos is not considered. Due to the fast rate of type I migration, the sweeping of 2:1 MMR (caused by type II migration of outside giant planets) and secular resonances may be lagged the fast inward migration of embryos, thus their effects will be greatly reduced. In that case, the embryos will migrate unless there are some mechanisms to stop it. Although in Fogg & Nelson 2007 they considered the type I migration in hot Jupiter systems, the formation of terrestrial planets in close-in orbits under the perturbations of giant planets in the outer region need to be re-investigated to see whether secular perturbations and secular resonances are effective.

Recent hydrodynamical simulations indicate that a location of density maximum in the gas disk can stop the type I inward migration (Masset et al. 2006). During the evolution of the protoplanet, the exchange of angular momentum between the protoplanet and the gas disk generates a corotation torque on the protoplanet with the expression (Ward 1991; Masset 2001; Masset 2002), $\Gamma_c \propto \Sigma_g d \ln(\Sigma_g/B)/d \ln a$, where Σ_g is the surface density of the gas disk, B is the Oort constant and $B \propto a^{-3/2}$ in a near Keplerian motion. If the surface density can

jump over 3 ~ 5 gas disk thickness, the positive corotation torque will overcome the negative Lindblad torque which causes the inward type I migration, making the location of density maximum a possible position to trap the protoplanets (Masset et al. 2006).

Several mechanisms can lead to the density maximum in the gas disk, e.g., *the inner disk cavity*. At the place where the torque induced by the stellar magnetic field dominates over disk internal stresses, material in the disk will fall onto the surface of the star thus the disk is truncated (Königl 1991). This place is roughly the corotation radius of the star, with a maximum stellar distance ~ 9 stellar radii. Before the protostar moving to the main sequence, the radius is 2-3 times larger. Thus the inner disk truncation of a main sequence star with mass $0.5 M_{\odot}$ is about 0.065 AU to 0.085 AU. In our simulations, we choose 0.1 AU as the boundary of the inner cavity of the gas disk. Once embryos reach this boundary, type I migration will be stopped effectively.

Near the *inner edge of the dead zone* (a_{crit}) is another location that induces density maximum in the gas disk. During the classical T Tauri star (CTTS) phase, inside a_{crit} , the protostellar disk is thermally ionized, so it is totally active zone. While outside a_{crit} , stellar X-rays and diffuse cosmic rays ionize a surface layer with a thickness $\cong 100 \text{ g cm}^{-2}$ on either side of the protostellar disk (active layer). Between the active layers is the dead zone near the midplane (Balbus & Hawley 1991; Gammie 1996). Near the inner edge of the dead zone in the midplane, a positive density gradient is induced (Kretke & Lin 2007; Kretke et al. 2009). For the protostellar disk in *ad hoc* α -prescription (Shakura & Sunyaev 1973), the mass accretion rate is constant across the disk, $\dot{M}_g = 3\pi\alpha c_s h \Sigma_g / \Omega_K$, where c_s and $h = c_s / \Omega_K$ are the sound speed of the midplane and the disk scale-height, respectively. As the value of α increases from dead zone (~ 0.006) to active zone (~ 0.018) (Sano et al. 2000), the gas density in the midplane of the disk increases from active zone to dead zone about two times. Then a density maximum appears in the inner edge of the dead zone which is helpful to halt the embryos undergoing type I migration.

Due to the density profile enhancement at the inner edge of magnetic inactive zone ($a_{crit} \sim 0.2 - 0.3 \text{ AU}$), embryos undergoing type I migration are expected to be stalled there, which makes the location around a_{crit} an ideal place for the accumulation of embryos. Cohesive mergers among embryos may finally form terrestrial planets. As the location of a_{crit} around dwarf stars with mass $\sim 0.5 M_{\odot}$ is roughly in the HZ, the forming planets may be most possibly habitable.

In this paper we study the formation of habitable planets due to the above mechanism with a model system OGLE-06-109L. Among the planets detected by microlensing, OGLE-06-109L system is the first one with observed multiple planets. It is 1490 pc away from the Sun, with a star of $\sim 0.51 M_{\odot}$ (solar mass) and two planets of $0.71 M_J$ (Jupiter mass) and $0.27 M_J$ in the orbits of 2.3 AU and 4.6 AU, respectively (Gaudi et al. 2008). The eccentricity of the out planet is 0.11 deduced from observation. In the first paper (Wang et al. 2009, hereafter WZZ09), we have studied the eccentricity formation of the system. The planetary scattering model

or the mean-motion resonance crossing model can be account for the eccentricity formation. According to our models, the final eccentricity of inner planet (e_b) may oscillate between [0-0.06], comparable to that of Jupiter (0.03-0.06).

According to Kasting et al. 1993, HZ is estimated to be [0.25-0.36 AU] or larger in OGLE-06-109L system. In WZZ09, we have demonstrated orbits in center of HZ with semimajor axis $a \in [0.28 \text{ AU}, 0.32 \text{ AU}]$ would be out of HZ due to the high eccentricities excited by the secular resonance of two giant planets in the system. An additional inner planet or outer planet would suppress the eccentricity perturbation and greatly improve the prospects for habitability of the system (Malhotra & Minton 2008). Orbits in the rest region of HZ remain in HZ up to 10 Myr integrations. Based on the results, OGLE-06-109L is a hopeful candidate system for hosting habitable terrestrial planets. The organizing of the paper is as follows. In section 2 we present the model, method and initial setup of the simulations. The simulation results are shown in Section 3. Section 4 presents our conclusions.

2. MODEL

2.1. Disk Model

To model the effect of density increment near a_{crit} in the gas disk, we formulate the gas disk as a viscous one with constant mass accreting to the star. Its surface density at stellar distance a is given as (Pringle 1981)

$$\Sigma_g = \frac{\dot{M}}{3\pi\nu(a)}, \quad (1)$$

where \dot{M} is the stellar accretion rate, $\nu(a)$ is the effective viscosity. According to the results from observation data of the young cluster ρ -Oph, the star accretion rate \dot{M} can be estimated to (Natta 2006)

$$\dot{M} \simeq 4 \times 10^{-8} \left(\frac{M_*}{M_{\odot}}\right)^{1.8} M_{\odot} \text{ yr}^{-1}. \quad (2)$$

So we adopt a baseline $\dot{M} = 1 \times 10^{-8} M_{\odot} \text{ yr}^{-1}$ for OGLE-06-109L system. However, during the earlier stage of T Tauri stage, \dot{M} could be 1-2 order of magnitude larger (Hartmann 2007).

The effective viscosity $\nu(a) = \alpha c_s h$, where α , c_s , and $h = c_s / \Omega$ refer to the efficiency factor of angular momentum transport, sound speed at the mid plane, and the isothermal density scale height, respectively (Shakura & Sunyaev 1973). To model this effect, we let α_{MRI} and α_{dead} denote the α -values of the MRI active and dead regions, respectively. The effective α for the disk is modeled as (Kretke & Lin 2007; Kretke et al. 2009)

$$\alpha_{eff}(a) = \frac{\alpha_{dead} - \alpha_{MRI}}{2} \left[\text{erf}\left(\frac{a - a_{crit}}{0.1a_{crit}}\right) + 1 \right] + \alpha_{MRI}, \quad (3)$$

where erf is the error function, $0.1a_{crit}$ is thought as the width of the transition region. In this paper, we adopt $\alpha_{MRI} = 0.01$, $\alpha_{dead} = 0.001$ (Sano et al. 2000). In all the simulations, we think the embryo to be run into the central star if its semimajor axis is less than 0.1 AU.

The location of the inner edge of the MRI dead zone, a_{crit} , varies with the disk temperature, kinematics and

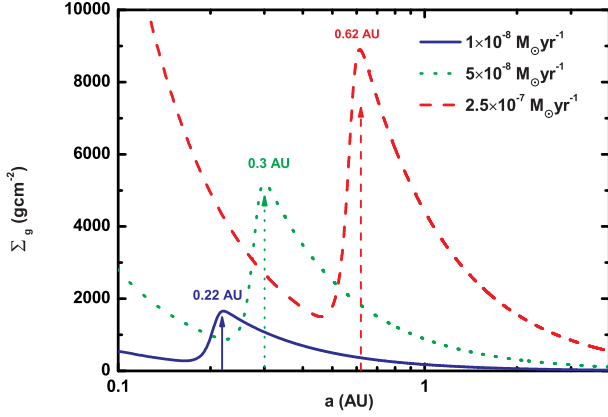


FIG. 1.— The density profile of the disk with different star accretion rate (\dot{M}). In the region outside the density maximum, the density profile satisfies $\Sigma_g \propto r^{-3/2}$. The blue solid line represents $\dot{M} = 1 \times 10^{-8} M_\odot \text{yr}^{-1}$, the location of the density maximum is at 0.22 AU. The green dot line shows the density profile of $\dot{M} = 5 \times 10^{-8} M_\odot \text{yr}^{-1}$, the density maximum location is at 0.3 AU. The red dash line means $\dot{M} = 2.5 \times 10^{-7} M_\odot \text{yr}^{-1}$, the location of the density maximum is at 0.62 AU. The inner edge of the disk is in the location of 0.1 AU.

mass accretion rate, etc. Here we adopt the expression from Kretke et al. (2009),

$$a_{\text{crit}} = 0.16 \text{ AU} \left(\frac{\dot{M}}{10^{-8} M_\odot \text{yr}^{-1}} \right)^{4/9} \left(\frac{M_*}{M_\odot} \right)^{1/3} \left(\frac{\alpha_{\text{MRI}}}{0.02} \right)^{-1/5}. \quad (4)$$

During the evolution of T-Tauri star and its disk, \dot{M} will decrease on average. So the location of a_{crit} is migrating inward as the time proceeds.

Combing with the empirical minimum mass solar nebula (hereafter MMSN, Hayashi 1981), we obtain the following surface density for the circumstellar disk (shown in Figure 1):

$$\Sigma_g = \Sigma_0 \left(\frac{a}{1 \text{ AU}} \right)^{-3/2} \left(\frac{\alpha_{\text{eff}}}{10^{-3}} \right)^{-1} \exp\left(-\frac{t}{\tau_{\text{dep}}}\right), \quad (5)$$

where $\Sigma_0 = 883 \text{ g cm}^{-2}$ is the initial density corresponding to that at $\sim 1 \text{ Myr}$ for $\dot{M} = 5 \times 10^{-8} M_\odot \text{yr}^{-1}$, due to disk accretion, photoevaporation or planet formation, the gas is depleted with a timescale $\tau_{\text{dep}} \sim 3 \text{ Myr}$ (Haisch et al 2001), t is the evolution time.

2.2. type I migration and e -damping

For a planet embedded in a geometrically thin and locally isothermal disk, angular momentum exchanges between the planet and the gas disk will cause a net momentum loss on the planet, which results in a fast and so-called type I migration of the planet (Goldreich & Tremaine 1979; Ward 1997; Tanaka et al. 2002). Some mechanisms are proposed recently to reduce the speed or even reverse the direction of migration. Laughlin et al. (2004), and Nelson & Papaloizou (2004) proposed that, in the locations where the magnetorotational instability (MRI) is active, gravitational torques arising from magnetohydrodynamical turbulence will contribute a random walk component to

the migratory evolution of the planets, thus prolong the drift timescale. Analytical estimation through Fokker Planck approach indicates the survival rate of planet under type I and stochastic torques is around 1 – 10% (Adams & Bloch 2009). Paardekooper & Mellema (2006) noticed that the inclusion of radiative transfer can cause a strong reduction in the migration speed. Subsequent investigations (Baruteau & Masset 2008; Kley & Crida 2008; Paardekooper & Papaloizou 2008) indicated that the migration process can be slowed down or even reversed for sufficiently low mass planets. Through full three-dimensional hydrodynamical simulations of embedded planets in viscous, radiative disks, Kley et al. (2009) confirmed that the migration can be directed outwards up to planet masses of about $33 M_\oplus$.

Taken these uncertainties into considerations, we adopt a standard description of type I migration with a speed reduction factor f_1 . The timescale of type I migration for an embryo m is (Tanaka et al. 2002)

$$\begin{aligned} \tau_{\text{migI}} &= \frac{a}{|\dot{a}|} \\ &= \frac{1}{f_1 (2.7 + 1.1\beta)} \left(\frac{M_*}{m} \right) \left(\frac{M_*}{\Sigma_g a^2} \right) \left(\frac{h}{a} \right)^2 \left[\frac{1 + \left(\frac{er}{1.3h} \right)^5}{1 - \left(\frac{er}{1.1h} \right)^4} \right] \Omega^{-1} \end{aligned} \quad (6)$$

where r, e, h, Ω , and Σ_g are the stellar distance, eccentricity of the embryo, scale height of the disk, the Kepler angular velocity, and the surface density profile of gas in the disk, respectively, $\beta = -d \ln \Sigma_g / d \ln a$. According to the density profile in equations (3) and (5), the factor β will be negative when crossing the location of density maximum to the inner disk. So when the embryo goes across the density maximum, the embryo may be sustained in the maximum location. In our simulations, we consider f_1 is in the range of [0.001, 1]. The type I migration effect is incorporated with an additional acceleration to any embryo with mass $\leq 10 M_\oplus$ (Cresswell & Nelson 2006),

$$\mathbf{F}_{\text{migI}} = -\frac{\mathbf{v}}{2\tau_{\text{migI}}}, \quad (7)$$

where \mathbf{v} is the velocity vector of m in the stellar-centric coordinate 2.

Interactions between embryos and the gas disk may damp the eccentricities of the embryos (Goldreich & Tremaine 1980). The timescale of the eccentricity damping for an embryo with mass $m < 10 M_\oplus$ can be described as (Cresswell & Nelson 2006),

$$\left(\frac{e}{\dot{e}} \right)_{\text{edap}} = \frac{Q_e}{0.78} \left(\frac{M_*}{m} \right) \left(\frac{M_*}{a^2 \Sigma_g} \right) \left(\frac{h}{r} \right)^4 \Omega^{-1} \left[1 + \frac{1}{4} \left(\frac{er}{h} \right)^3 \right], \quad (8)$$

where r, e, h, Ω are the distance from the star, eccentricity of the embryo, scale height of the disk and the Kepler angular velocity, respectively, $Q_e = 0.1$ is a normalization factor to fit with hydrodynamical simulations. This effect is included by add an extra-force term to the equations of embryo motion:

$$\mathbf{F}_{\text{edap}} = -2 \frac{(\mathbf{v} \cdot \mathbf{r}) \mathbf{r}}{r^2 \tau_{\text{edap}}}. \quad (9)$$

2.3. Initial configurations of the system

We assume two giant planets (m_b, m_c) have already formed with observed masses of OGLE-09-106L b, c initially at 4 AU and 8 AU, respectively. The giant planets

undergo type II migration with a fixed timescale about 1 Myr (WZZ09). An additional embryo with mass $16.8 M_{\oplus}$ is put between them. A planetary scatter will occur between one giant planet and the additional embryo at about 5 Myr, just as in WZZ09, to account for the observed eccentricities of the two giant planets.

To model the formation of planets in the terrestrial region, we put 18 embryos with isolation masses (Ida & Lin 2004)

$$M_{\text{iso}} = 0.12 \gamma_{\text{ice}}^{3/2} f_d^{3/2} \left(\frac{a}{1 \text{ AU}}\right)^{3/4} \left(\frac{M_*}{M_{\odot}}\right)^{-1/2} M_{\oplus} \quad (10)$$

in the inner region, where γ_{ice} is the volatile enhancement with a value of 4.2 or 1 for material exterior or interior to the snow line (0.68 AU for OGLE-06-109L system), respectively. The embryos with the isolation mass are located in 10 mutual Hill radii from each other. For a dwarf star with mass $0.51 M_{\odot}$, we assume a disk with $f_d \leq 2$. For $f_d = 1$, the masses of embryos range from $0.084 M_{\oplus}$ to $3.33 M_{\oplus}$ at [0.39 AU, 3 AU], with a total mass of $19.1 M_{\oplus}$. For $f_d = 2$, the masses of embryos range from $0.175 M_{\oplus}$ to $9.42 M_{\oplus}$ at [0.26 AU, 3 AU], with a total mass of $38.5 M_{\oplus}$. The outmost embryo in the inner region is in the orbit 3.5 Hill Radii away from m_b . The giant planets and embryos are all in near-coplanar and near-circular orbits initially (with initial eccentricities $e = 10^{-3}$ and inclinations $i = e/2$).

2.4. Perturbation from two giant planets

The effect of giant planets is twofold: for embryos in nearby orbits, perturbations from two giant planets will excite their eccentricities, which may be helpful for the merge of small embryos into ones. The maximum eccentricity that an embryo initially in circular orbits exited under the perturbation of out planet is (Mardling 2007)

$$e_{\text{max}} = \frac{(5/2)(a_e/a_c)e_c\epsilon^{-2}}{\left|1 - \sqrt{a_e/a_c}(m_e/m_c)\epsilon^{-1}\right|}, \quad (11)$$

where subscribes of e and c denote those of the embryo in inner orbit and the giant planet, respectively, $\epsilon = \sqrt{1 - e_c^2}$. According to equation (11), the excitation of initial embryos located from [0.26, 3] AU is [0.01, 0.10] from m_b and [0.007, 0.08] from m_c . Thus the effect of inner giant planet is non-negligible for embryos around 3 AU.

Another effect that may contribute to the formation of planets in habitable region is the secular resonance. Due to the presence of gas disk and mutual perturbation, the orbits of two giant planets will precess with eigenfrequencies (s_1, s_2) (Heppenheimer 1980),

$$s_{1,2} = \frac{1}{2} \{ (A_{11} + A_{22}) \pm [(A_{11} - A_{22})^2 + 4A_{12}A_{21}]^{1/2} \}, \quad (12)$$

where

$$\begin{aligned} A_{11} &= 2n_b a_b m_c N_{bc} - (\pi F / 4a_b) \sigma_0, \\ A_{12} &= -2n_b a_b m_c P_{bc}, \\ A_{22} &= 2n_c a_c m_b N_{bc} - (\pi F / 4a_c) \sigma_0, \\ A_{21} &= -2n_c a_c m_b P_{bc}, \end{aligned}$$

where $\sigma_0 = \Sigma_0(\alpha_{\text{eff}}/10^{-3})^{-1} \exp(-t/\tau_{\text{dep}})$. We define $a_- = \min(a_b, a_c)$ and $a_+ = \max(a_b, a_c)$, so that

$$\begin{aligned} N_{bc} &= \frac{1}{8} (a_-/a_+^2) b_{3/2}^{(1)} (a_-/a_+), \\ P_{bc} &= \frac{1}{8} (a_-/a_+^2) b_{3/2}^{(2)} (a_-/a_+), \end{aligned}$$

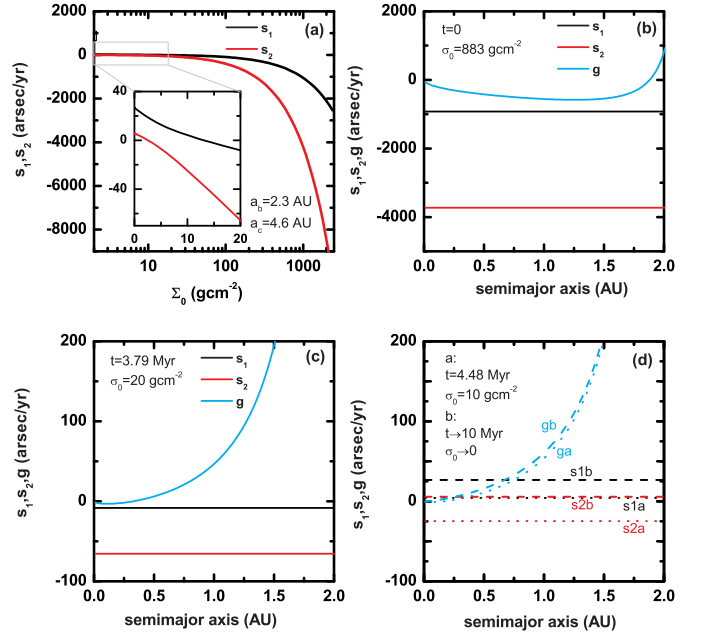


FIG. 2.— Location of secular resonance in the inner region of the system at different time during the evolution. (a) The precession eigenfrequencies s_1, s_2 of the two giant planets due to different density of gas disk Σ_0 and mutual perturbation. (b) At $t=0$, the proper frequency of test particle g compared to s_1, s_2 . There is no point of intersection between g and s_1, s_2 . Secular resonance cannot happen in the inner region of the system. (c) At $t=3.76$ Myr, the proper frequency of test particle g compared to s_1, s_2 . g is close to s_1 . (d) At $t=4.48$ Myr and 10 Myr, the proper frequency of test particle g compared to s_1, s_2 . Secular resonance happens at the location of ~ 0.25 AU.

where $b_{3/2}^{(i)}$ is the Laplace coefficients. $F = 4.377345$ for surface density slope $\beta = 3/2$.

The proper frequency of test particle associated with the longitude of perihelion is

$$g = 2n_p a_p \cdot (m_b N_{pb} + m_c N_{pc}) - (\pi F / 4a_p) \sigma_0, \quad (13)$$

where subscript p refers to the test particle, terms with N_{pb}, N_{pc} are due to the perturbation of two planets, term with σ_0 is due to the gas disk. The definition of N_{pb} and N_{pc} are similar to N_{bc} . When the proper frequency of an embryo meets with either of the two eigenfrequencies, i.e., $g = s_i$ ($i=1, 2$), secular resonance occurs, which may excite the eccentricities of embryos.

The two eigenfrequencies (s_1, s_2) are plotted in Figure 2a. As we can see, the orbits of two planets precess retrogradely ($s_i < 0$) unless the gas disk is almost depleted ($\sigma_0 \leq 10 \text{ gcm}^{-2}$), so the procession rate is slow (with period > 2000 yr) and prograde. Also the precession frequency g located inside 2.0 AU does not equal to s_1, s_2 unless $\Sigma_g < 20 \text{ gcm}^{-2}$ (Figure 2b-d). This occurs when $t > 3.8$ Myr. At $t = 10$ Myr, the gas disk is effectively depleted, either s_1 or s_2 may meet g at some locations of habitable zone. As the secular resonances at habitable zone occurred only at the epoch when the gas disk is almost depleted, we omit the effect of self gravity of gas disk in the following simulations.

3. SIMULATIONS AND RESULTS

We numerically integrate the full equations of planet motions with a time-symmetric Hermit scheme (Aarseth 2003). Regularization technique is used to handle the collision between embryos, so all the embryos have their physical radii. As long as the mutual distance between two embryos is smaller than the sum of their physical radius, we assume they are merged.

We perform four Groups of simulations with different star accretion rate (\dot{M}) and the heavy element scaling factor with respect to the MMSN model (f_d), see Equation (10). In our simulations we choose $\dot{M} = 1 \times 10^{-8}$, 5×10^{-8} , and $2.5 \times 10^{-7} M_\odot/\text{yr}$, corresponding to different stages of T Tauri stars so that higher \dot{M} corresponds to earlier stage. The conditions in different Groups are listed as follows:

Group 1 : $f_d = 2$; $\dot{M} = 5 \times 10^{-8} M_\odot/\text{yr}$ responds to the green dot line in figure 1.

Group 2 : $f_d = 2$; $\dot{M} = 1 \times 10^{-8} M_\odot/\text{yr}$ responds to the blue solid line in figure 1.

Group 3 : $f_d = 2$; $\dot{M} = 2.5 \times 10^{-7} M_\odot/\text{yr}$ responds to the red dash line in figure 1.

Group 4 : $f_d = 1$; $\dot{M} = 5 \times 10^{-8} M_\odot/\text{yr}$ responds to the green dot line in figure 1.

We perform 31 runs with the same disk model except varying f_1 from 0.001 to 1 in each Group. The results are presented as follows.

3.1. Formation and orbital configurations of terrestrial planets

One of the most important factors that affects the formation of planets in habitable zone is the speed of type I migration reduced by f_1 . If the speed is very slow, the embryos will not migrate too much. Fig.3 shows a typical run of Group 1 with very low migration speed ($f_1 = 0.004$). Planetary mergers mainly occur due to scattering effect of embryo inside two giant plants at $t \sim 5$ Myr (WZZ09). As we know from the density profile in Figure 1, when $\dot{M} = 5 \times 10^{-8} M_\odot/\text{yr}$, the location of density maximum is at 0.3 AU. At this density maximum, the type I migration of embryos can be stalled due to the negative β in equations (6). The inward migration of a second planet may trap the stalled planet into its mean motion resonance, which might increase the eccentricities of both planets. As we can see, most of the planets survived at $t = 10$ Myr with $a < 1$ AU are trapped into first order resonance (mainly 4:3). Among them, one is in the HZ and two of them are at the edge of the HZ in this case.

With the increase of the type I migration speed, less and less embryos are survived or trapped in HZ before the gas disk was almost depleted. For example, Figure 4 shows a typical run with migration reduced factor $f_1 = 0.08$. Only two terrestrial planets survived at the inner region ($a < 1$ AU). Interestingly, they are in 2:1 MMR. The inner planet with mass ($7.5 M_\oplus$) is in the HZ. As the migration speed increases again, $f_1 = 0.25$, only one planet survived in the HZ (Figure 5a). It is stalled under

type I migration at the inner edge of MRI dead zone (Figure 5b).

According to Figure 3b, many planet pairs may be trapped in MMRs under migration. Table 1 shows the statistics of the final configurations for the simulations in the four Groups. We classify the system being in either MMRs, aligned apsidal resonance (AARs) or anti-aligned apsidal resonance (anti-AARs) if there is at least one couple of planets trapped into MMRs, AARs or anti-AARs. Table 1 records the probability of a planet system that is in MMRs, AARs or anti-AARs in the 31 runs of each group (24 runs in Group 3). As we can see, more than a quarter of the systems contain at least a planet pair that is in MMRs, AARs or anti-AARs.

3.2. Stable time of the system

For systems with only one terrestrial planet, we can get the stable time from the results in WZZ09. Because the distance of the single terrestrial planet to the central star is closer than 0.56 AU in our results. All the single terrestrial planets systems are stable in more than 10^8 years. Based on Zhou et al. (2007) about the crossing time of planet system, we estimate the stable time of multiple terrestrial planet system at the end of the simulations. We test each couple of the planets in the systems and use the average eccentricity, average mass and relative Hill radius for the two planets next to each other in the estimation. Results are showed in table 2. More than 60% couples of the planets in the system will survive in more than 10^8 years. According to the results of the stable time of the planets, we get the stable time of the planetary system. We define the shortest time of the planet couples surviving in the system as the stable time of the system. The results are also showed in the last column of table 2. More than 41% system will be stable in more than 10^8 years.

3.3. Water contents of terrestrial planets

For terrestrial planets in habitable zone, one important parameter is the water content inside the rock. To model the distribution of water contents within embryos, we initially assume the inner disk is water-poor, embryo within 0.5 AU is 0.001% by mass, while embryo beyond 0.625 AU is wet with the water content 5%, embryo between them is moderately wet with 0.1% water. We further assume, the water content will be decreased by 30% during each collision (Melosh 2003). Thus the migration and merge of embryos may re-distribute the water contents.

Figure 6 shows the simulation results of Group 1. The color map represents the water distribution by mass (Raymond et al. 2004). Panel (a1) and (b1) show the distribution of the habitable planets changed with f_1 . If type I migration of the embryos are fast, $f_1 > 0.2$, most of the small embryos originally in the HZ were run into the central star, the only survival planet with high mass ($\sim 7 M_\oplus$) was migrated from outside (> 2.2 AU). So they have relative high water contents. When $f_1 < 0.07$, the slow migration of embryos are easily to be perturbed by either the secular perturbations or secular resonance induced by the two giants. So planetary merges occurred occasionally, and the motion of the embryos are chaotic. As planetary merges reduce the water contents of the rocks, such formed planets with masses $> 7M_\oplus$ are drier than neighbor embryos .

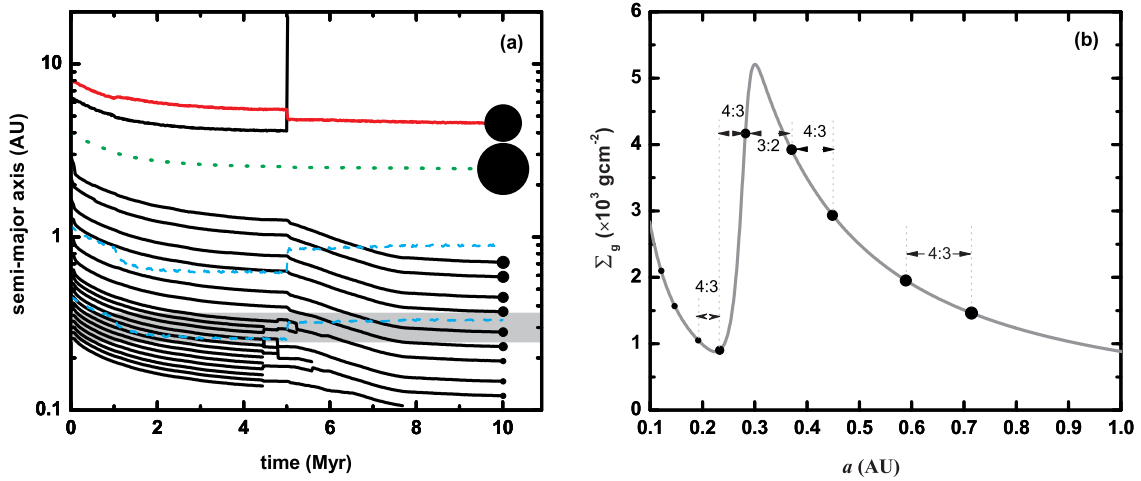


FIG. 3.— A typical run with $f_1 = 0.004$ in Group 1. There are nine terrestrial planets with masses less than $7M_{\oplus}$ left in the system. One is in the HZ and two of them are at the edge of the HZ. At the end of the simulation they trapped into 4:3 and 3:2 MMRs respectively. (a) Evolution of the semi-major axes. The gray band represents the HZ and the two blue dashed lines indicate the location of secular resonance caused by the giant planets. (b) The final locations of the terrestrial planets in the system. The ordinate of each planet is chosen to fit the gas density profile for illustrative purposes. MMRs are labeled.

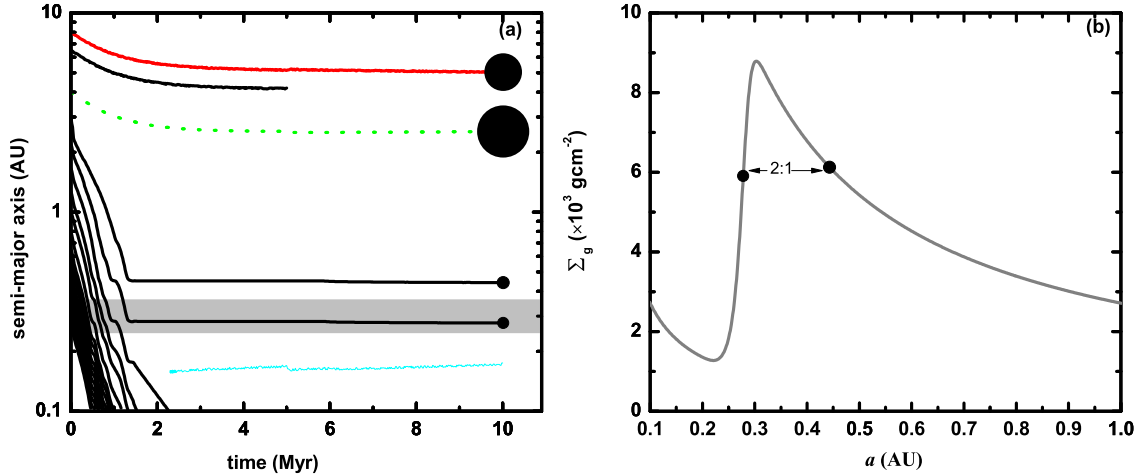


FIG. 4.— A typical run with $f_1 = 0.08$ in Group 1. There are two terrestrial planets left in the system. One is in the HZ. At the end of the simulation they trapped into 2:1. (a) Evolution of the semi-major axes. The gray band represents the HZ and the blue dashed line indicates the location of secular resonance caused by the two giant planets and the other terrestrial planet. (b) The final locations of the terrestrial planets in the system. The ordinate of each planet is chosen to fit the gas density profile for illustrative purposes.

TABLE 1

STATISTIC OF THE FINAL CONFIGURATIONS OF THE SIMULATIONS IN THE FOUR GROUPS. F-Pb AND F-Pc SHOW THE FINAL AVERAGE LOCATIONS AND ECCENTRICITIES OF GIANT PLANET B AND C RESPECTIVELY. F-MMRs IS THE PROBABILITIES OF PLANETS (IN ALL PLANETS) AND THE SYSTEM (WITH AT LEAST ONE PLANET PAIR) CAPTURED INTO MMRs. WE CONSIDER THE SYSTEM IS IN MMRs IF THERE IS AT LEAST ONE COUPLE OF PLANETS TRAPPED INTO MMRs. F-AAR AND F-ANTI AAR ARE THE STATISTIC OF THE PLANETS AND SYSTEMS TRAPPED INTO ALIGNED APSIDAL RESONANCE AND ANTIALIGNED APSIDAL RESONANCE IN THE FINAL CONFIGURATIONS.

ID	f-Pb	f-Pc	f-MMRs	f-AAR	f-antiAAR
	a (AU), e	a (AU), e	Planet, System	Planet, System	Planet, System
G1	2.474, 0.076	5.267, 0.108	63.4%, 17/31	62.7%, 18/31	56.2%, 15/31
G2	2.547, 0.087	5.272, 0.132	47.6%, 16/31	48.4%, 12/31	48.4%, 16/31
G3	2.486, 0.065	5.166, 0.101	30.8%, 7/24	46.2%, 6/24	27.4%, 6/24
G4	2.000, 0.087	5.040, 0.107	23.0%, 11/31	56.0%, 13/31	41.0%, 13/31

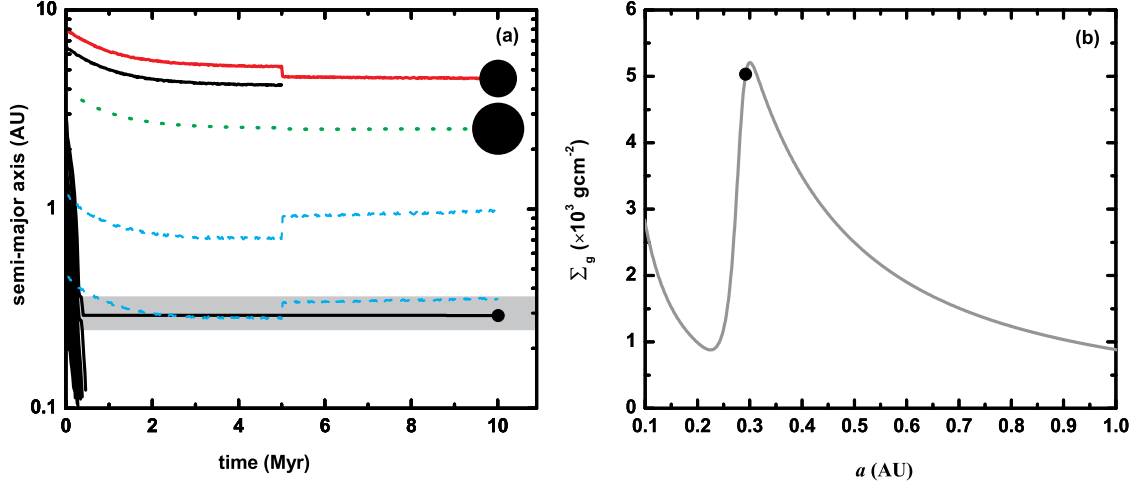


FIG. 5.— A typical run with $f_1 = 0.25$ in Group1. There is one terrestrial planet left in the system and it is in the habitable zone. (a) Evolution of the semi-major axes. The gray band represents the HZ and the two blue dashed lines indication the location of secular resonance caused by the two giant planets. (b) The final location of the terrestrial planet in the system. The ordinate of the planet is chosen to fit the gas density profile for illustrative purposes.

TABLE 2

STATISTIC OF THE STABLE TIME OF THE MULTIPLE TERRESTRIAL PLANET SYSTEMS. THE FIRST THREE COLUMNS MEANS THE STATISTIC OF THE PLANET COUPLES AND THE LAST COLUMN REPRESENTS THE RESULTS OF THE PLANETARY SYSTEMS IN EACH GROUP.

ID	$> 10^6$ yr	$> 10^7$ yr	$> 10^8$ yr	system stable time $> 10^8$ yr
G1	92.6%	84.4%	63.9%	41.67%
G2	90.4%	86.2%	69.1%	47.82%
G3	91.1%	83.3%	77.8%	50%
G4	92.8%	92.8%	87%	75.86%

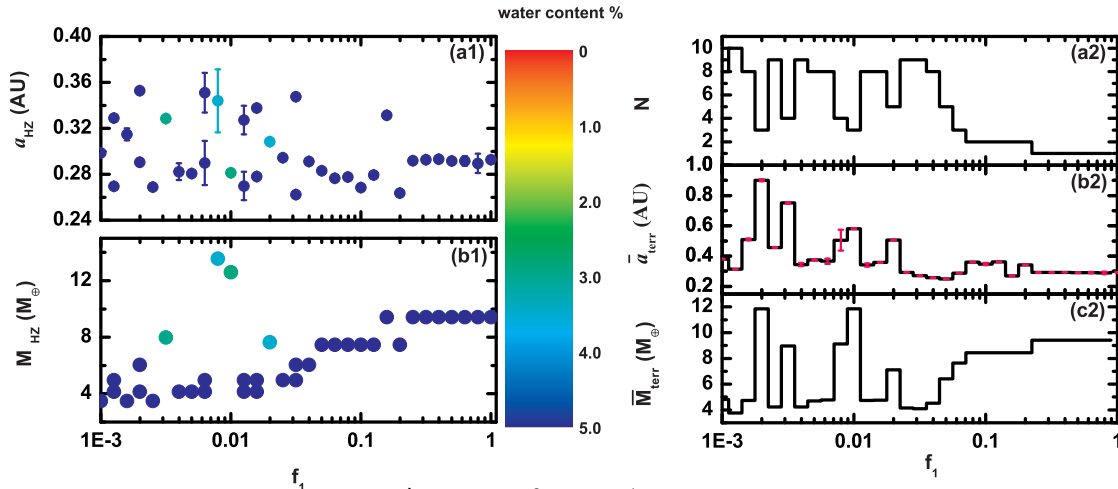


FIG. 6.— The results of Group 1 with $\dot{M} = 5 \times 10^{-8} M_{\odot} yr^{-1}$ at the end of our simulations ($t=10$ Myr). (a1): The semimajor axes of the habitable planets distribution changed with f_1 . (b1): The Mass of the habitable planets distribution. (a2): The number of the terrestrial planets survived in the system. (b2) The average semimajor axes of terrestrial planets distribution changed with f_1 . (c2) The average masses of the terrestrial planets distribution. The color map in the left panels represents the water distribution by mass. The error bars in Panel (a1) and (b2) show a(1-e) and a(1+e).

Panels (a2), (b2), and (c2) of Figure 6 are the distribution of the terrestrial planets. From Figure 6a2, if the type I migration speed is slow, there will be many embryos left in the inner region. $f_1 \sim 0.1$ is the critical value f_{1crit} above which only one or two terrestrial planets formed and survived in the system. The average semi-major axes of the terrestrial planets showed in Panel (b2) are small when $f_1 \geq 0.1$, within the snowline (0.68 AU in OGLE-06-109L system), so most of the terrestrial planets keep in the inner region of the system. As it's possible to form planets with mass $> 10 M_\oplus$, they might have the chance to accretion gas and form Neptune-size planets if there is still enough gas in the disk.

In Group 2 and 3, we change the star accretion rate to $\dot{M} = 1 \times 10^{-8} M_\odot/\text{yr}$ and $\dot{M} = 2.5 \times 10^{-7} M_\odot/\text{yr}$ respectively. This corresponds to the formation of terrestrial planet occurred either later or earlier so that the mass accretion rate of the star is either smaller or larger. Figure 7 shows the results of the two groups. When $f_1 > 0.1$ of Group 2, there are one or two planets left in the system, and the inner most terrestrial planet with mass $\sim 9.4 M_\oplus$ locates around 0.22 AU, the density profile maximum around the HZ. For Group 3, $\dot{M} = 2.5 \times 10^{-7} M_\odot/\text{yr}$, the location of density maximum is 0.62 AU. There is no terrestrial planet left in the system for $f_1 > 0.2$.

From Figure 7c1 and c2, we can get that if $f_1 \leq 0.1$, there are more than one terrestrial planets survival in the system. It also agrees with the result of Terquem & Papaloizou (2007) that the hot super-Earths or Neptunes formed by mergers of inwardly migrating cores are most likely not isolated. The average semimajor axes in Figure 7d1 and d2 show that most of the terrestrial planets are distributed inside the snowline (0.68 AU). The water content in the region of $f_1 < 0.1$ is lower than that of $f_1 > 0.1$, in which case the terrestrial planets are mainly from outside orbits with high water contents.

Figure 8 shows the results of Group 4 for the embryos with $f_d = 1$. Because f_d is related to the mass of the embryos initially, the mass of the habitable planets will be smaller than other Groups. From the timescale of type I migration, equation (6), the migration speed is in proportion to $f_1 \times m$. So when $f_d = 1$, the migration is slower than the runs in other Groups. In Group 4, if f_1 is less than 0.2, most of the habitable planets left in the system are merged from small embryos for several times. The water contents of the planets are low. When $f_d = 1$, the initial masses of all embryos are less than $3.3 M_\oplus$. At last the average mass of Group 4 is about $4 M_\oplus$. The habitable planet whose mass higher than $7 M_\oplus$ is formed from merge with low water content. In this Group, there are more than one terrestrial planets survival in the range of $f_1 \in [0.001, 1]$.

4. CONCLUSIONS AND DISCUSSIONS

In this paper, we investigate the formation of terrestrial planets under the perturbation of giant planets around dwarf stars, with a model system OGLE-06-109L. We assume two giant planets already formed in outside orbits. The embryos are initially embedded in an exponentially decaying gas disk and will under type I migration with a speed reducing factor f_1 over the standard (linear) estimation. The presence of giant planets may excite the eccentricities of embryos in nearby orbits through secular perturbations, and induce secular resonance in the hab-

itable zone regions when the gas disk is almost depleted.

The speed of type I migration plays an important role in determine the number and orbital architecture of terrestrial planets. When $f_1 \leq 0.1$ (0.1 times of the standard speed), there may be several terrestrial planets formed in the inner region (< 1 AU). Massive terrestrial planets formed by mergers of smaller mass embryos, thus they have lower water contents compared with neighboring embryos with small masses. Some of the planet pairs are trapped either in MMRs, or AARs or anti-AARs. The formation of planets in MMR is due to the halt of inner planets at the inner edge of MRI dead zone, or due to the convergent migration during the evolution. According to our simulations, most of the formed MMRs are first order resonances which have wider resonance regions. In the case that type I migration speed is fast ($f_1 > 0.1$), there will be very few (or sometimes no) terrestrial planets in the inner region. They are mainly migrated from outer regions so they have higher water contents as compared with neighboring embryos. Thus through the water contents of the terrestrial planets, we can deduce their origin.

The change of star accretion rate reflects the location of the density maximum, which affects the survival of the planets in the habitable region [0.25, 0.36] AU in OGLE-06-109L system. If the giant embryos in the inner region (< 1 AU) of the system formed in the earlier (for example, Figure 7a2-e2, $\dot{M} = 2.5 \times 10^{-7} M_\odot/\text{yr}$), the surface density of the disk is still high so that the high speed type I migration (with $f_1 > 0.1$) may drive all the embryos into the star. Only lower speed migration and later formed embryos are easier to retained. However, the model of type I migration described by equations (6) and (7) are linear. When more realized model is considered, e.g., considering the outward migration in viscous, radiative disks (Kley et al. 2009), things will be more complicated and interesting.

Another important factor is the initial conditions of the embryos. In our simulations, the embryos we used are in isolation masses. In order to test the reasonability of the initial conditions, we run with more embryos with smaller initial masses using $f_1 = 0.004$. Figure 9 shows the result. Finally, we get a planet with mass of $4.4 M_\oplus$ in the habitable zone which is comparable to the result in figure 3. And the system will be stable in more than 10^8 years. We test other runs and find that the results are similar to the run when $f_1 = 0.004$. So our results with the embryos in isolation mass initially are reasonable.

According to our simulations, by checking the water contents of terrestrial planets in OGLE-06-109L (and other similar systems), one can understand their formation history, and also restrict the parameters such as f_1 used in the planetary formation theory. For the OGLE-06-109L system, the snowline is about 0.68 AU, very close to the central star. If one or no terrestrial planet is observed, basically they might formed through inward migration from outside the snow line, thus they will have relatively high water contents ($\sim 0.5\%$), also the type I migration speed is fast ($f_1 > 0.1$). If many planets are observed in the inner region (< 1 AU), then most probably, they are formed through merges of isolation cores, thus they will have relatively low water contents $\sim 2\%$. The presence of multiple terrestrial planets also indicates

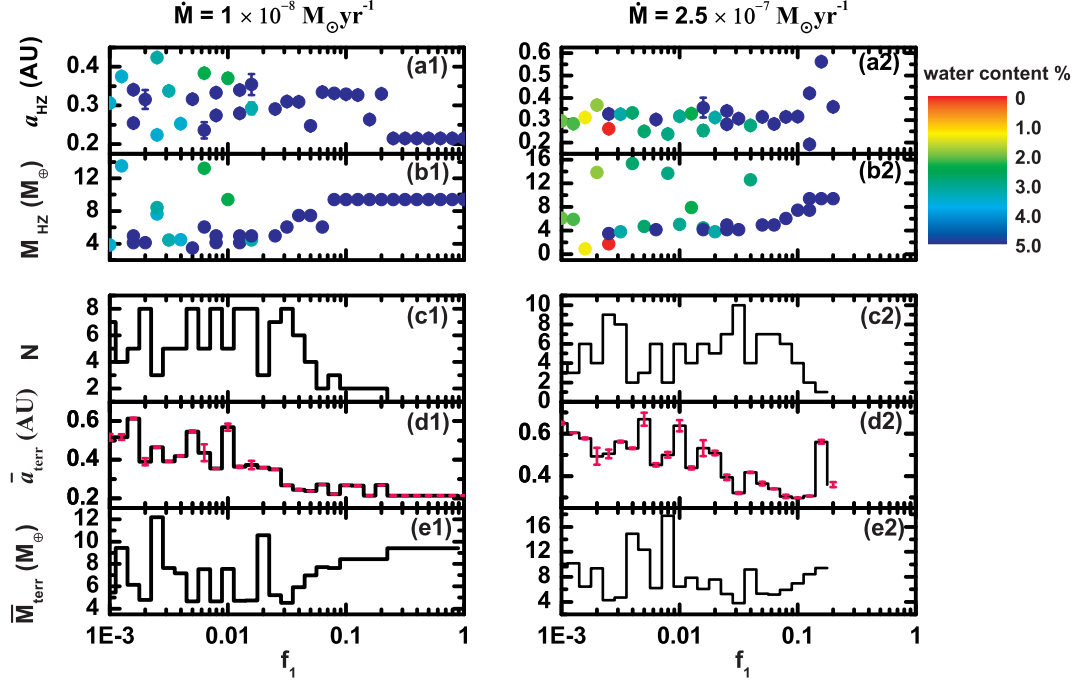


FIG. 7.— The results of Group 2 (left panels) and Group 3 (right panels) at the end of our simulations ($t=10$ Myr). Panel (a1) and (b1) are the semimajor axes and mass distribution of the habitable planets in Group 2 with $\dot{M} = 1 \times 10^{-8} M_{\odot} \text{yr}^{-1}$. Panel (c1), (d1), and (e1) are the number, average semimajor axes, and average mass distribution of the terrestrial planets in Group 2. Panel (a2) and (b2) are the results of habitable planets in Group 3 with $\dot{M} = 2.5 \times 10^{-7} M_{\odot} \text{yr}^{-1}$. Panel (c2), (d2), and (e2) are the results of terrestrial planets of Group 3. The error bars in panel (a1), (a2), (d1), and (d2) show $a(1-e)$ and $a(1+e)$.

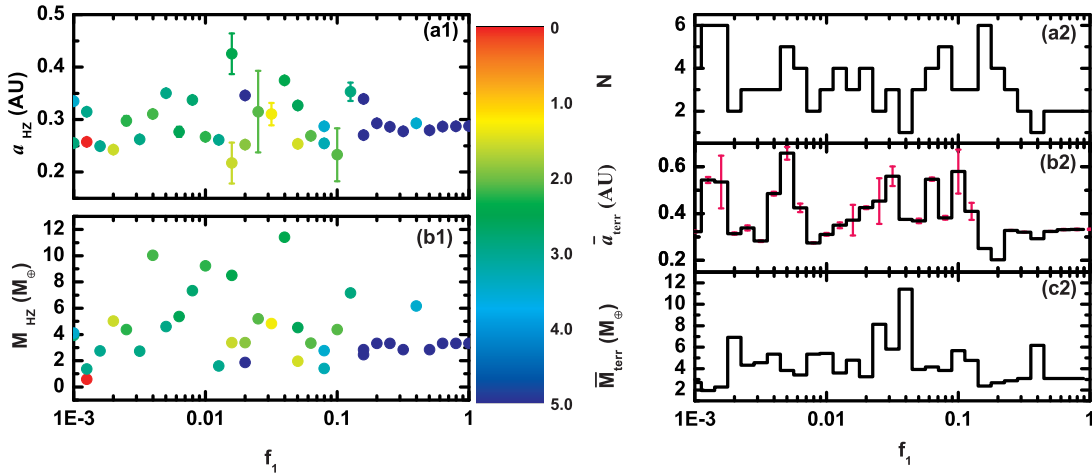


FIG. 8.— The results of Group 4 at the end of our simulations ($t=10$ Myr). Panel (a1) and (b1) are the habitable planets distribution of Group 4 with $f_d = 1$. Panel (a2), (b2), and (c2) are the results of terrestrial planets in Group 4. The error bars in Panel (a1) and (b2) show $a(1-e)$ and $a(1+e)$.

a low speed migration of the embryos ($f_1 < 0.1$).

This work is supported by NSFC (10925313, 10833001, 10778603), National Basic Research Program of China

(2007CB814800) and Doctoral Funds of Universities (20000091110002).

REFERENCES

- Aarseth, S. J. 2003, Gravitational N-Body Simulations, Cambridge University Press, Cambridge.
- Adams, F. C., & Bloch, A. M. 2009, ApJ, 701, 1381
- Balbus, S. A., & Hawley, J. F. 1991, ApJ, 376, 214
- Baruteau, C., & Masset, F. 2008, ApJ, 672, 1054
- Cresswell, P., & Nelson, R. P. 2006, A&A, 450, 833
- Fogg, M. J., & Nelson, R. P. 2005, A&A, 441, 791
- Gammie C. F. 1996, ApJ, 457, 355
- Gaudi, B. S., et al. 2008, Science, 319, 927
- Goldreich, P., & Tremaine, S. 1979, Icarus, 233, 857

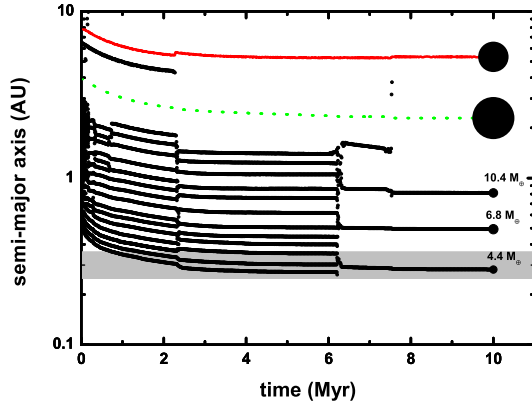


FIG. 9.— The results with different initial conditions. In this run, we use 90 embryos in $0.4 M_{\oplus}$ initially. Finally, we get a planet with mass of $4.4 M_{\oplus}$ in the habitable zone which is comparable to the result in Figure 3.

Goldreich, P., & Tremaine, S. 1980, *ApJ*, 241, 425
 Haisch, K. E., Lada, E. A., & Lada, C. J. 2001, *ApJ*, 553, L153
 Hartmann, L. 2007, *Accretion Processes in Star Formation*, Cambridge University Press, Cambridge.
 Hayashi, C. 1981, *Prog. Theor. Phys. Suppl.*, 70, 35
 Heppenheimer, T. A. 1980, *Icarus*, 41, 76
 Hinse, T. C., Michelsen, R., Jorgensen, U. G., Gozdziewski, K., & Mikkola, S. 2008, *A&A*, 488, 1133
 Ida, S., & Lin, D. N. C. 2004, *ApJ*, 604, 388
 Kasting, J. F., Whitmire, D. P., & Reynolds, R. T. 1993, *Icarus*, 101, 108
 Kley, W., & Crida, A. 2008, *A&A*, 487, L9

Kley, W., Bitsch, B., & Klahr, H. 2009, *A&A*, 506, 971K
 Königl, A. 1991, *ApJ*, 370, L39
 Kretke, K. A., & Lin, D. N. C. 2007, *ApJL*, 664, 55
 Kretke, K. A., Lin, D. N. C., Garaud, P., & Turner, N. J. 2009, *ApJ*, 690, 407
 Laughlin, G., Steinacker, A., & Adams, F. C. 2004, *ApJ*, 608, 489
 Malhotra, R., & Minton, D. A. 2008, *ApJL*, 683, 67
 Mardling R. A. 2007, *MNRAS*, 382, 1768
 Masset, F. S. 2001, *ApJ*, 558, 453
 Masset, F. S. 2002, *A&A*, 387, 605
 Masset, F. S., Morbidelli, A., Crida, A., & Ferreira, J. 2006, *ApJ*, 642, 478
 Melosh, H. J. 2003, *Nature*, 424, 22
 Nagasawa, M., Lin, D. N. C., & Ida, S. 2003, 586, 1374
 Natta, A., Testi, L., & Randich, S. 2006, *A&A*, 452, 245
 Nelson, R. P., & Papaloizou, J. C. B. 2004, *MNRAS*, 350, 849
 Paardekooper, S. -J., & Mellema, G. 2006, *A&A*, 459, L17
 Paardekooper, S. -J., & Papaloizou, J. C. B. 2008, *A&A*, 485, 877
 Pringle, J. E. 1981, *ARA & A*, 19, 137
 Raymond, S. R., Quinn, T., & Lunine, J. I. 2004, *Icarus*, 168, 1
 Raymond, S. N., Mandell, A. M., & Sigurdsson, S. 2006, *Science*, 313, 1413
 Raymond, S. N., Barnes, R., & Mandell, A. M. 2008, *MNRAS*, 284, 663
 Sano, T., Miyama, S. M., Umebayashi, T., & Nakano, T. 2000, *ApJ*, 543, 486
 Shakura, N. I., & Sunyaev, R. A. 1973, *A&A*, 24, 337
 Tanaka, H., Takeuchi, T., & Ward, W. R. 2002, *ApJ*, 565, 1257
 Terquem, C., & Papaloizou, J. C. B. 2007, *ApJ*, 654, 1110
 Ward, W. R. 1991, *Lunar Planet Sci. Conf.*, 22, 1463
 Ward, W. R. 1997, *Icarus*, 126, 261
 Wang, S., Zhao, G., & Zhou, J. L. 2009, *ApJ*, 706, 772 (WZZ09)
 Zhou, J. L., Aarseth, S. J., Lin, D. N. C., & Nagasawa, M. 2005, *ApJL*, 631, 85
 Zhou, J. L., Lin, D. N. C., & Sun, Y. S. 2007, *ApJ*, 666, 423